Modeling of Casting, Welding and Advanced Solidification Processes - XI
Edited by Charles-André Gandin and Michel Bellet
TMS (The Minerals, Metals & Materials Society), 2006

VOLUME AVERAGING CONCEPT FOR MIXED COLUMNAR-EQUIAXED SOLIDIFICATION

M. Wu and A. Ludwig

Simulation and Modeling of Metallurgical Processes, Dept. of Metallurgy
University of Leoben, A-8700, Austria

Keywords: Columnar-to-Equiaxed Transition, Convection, Sedimentation, Macrosegregation.

Abstract

A 3-phase volume averaging model is developed for mixed columnar-equiaxed solidification. The three phases are the melt, the solidifying columnar dendrites and equiaxed grains. As the numerical method and solution procedure for the multiphase volume averaging approach were presented previously, this paper focuses on the formulations of the model of mixed columnar-equiaxed solidification, and on the algorithm for predicting the CET. Different formulations for the equiaxed and the columnar volume-averaged mass transfer rates based on diffusion controlled growth models are proposed. Dendrite tip growth kinetics is applied to determine the columnar tip position. A new algorithm is developed to track the columnar dendrite tip front. In addition to the competitive growth between equiaxed grains and columnar dendrites, the mechanical interaction between them is simplified: the equiaxed grains are allowed to move freely near the columnar tips, whereas within the interdendrite region they are ‘captured’ by the growing columnar dendrites. The columnar tip stop mechanism proposed by J.D. Hunt is implemented to predict the CET. A 3D benchmark ingot (Fe-0.34 wt% C) is simulated to show the potentials of the model. 1D simulations with corresponding assumptions were also carried out to evaluate the recent model by comparing it with classical analytical solutions.

Introduction

With present-day computing resources, two methods are considered suitable for mixed columnar-equiaxed solidification of castings at an industrial scale including CET: deterministic models based on the volume averaging concept [1-2], and stochastic models based on e.g. the cellular automaton [3-5]. However, all the CET models developed up till now did not properly account for the effect of melt convection and grain sedimentation. Recently, the authors presented a 2-phase deterministic model for equiaxed solidification [6-8]. The recent 3-phase model is an extension of this model, which now also includes the stationary columnar phase, and interactions between the stationary phase and the moving equiaxed phase.

The Mixed Columnar-Equiaxed Solidification Model

Three phases are considered: the melt (*l*) as a primary phase, the equiaxed (*e*) and columnar (*c*) as secondary phases. All 3 phases are treated as interpenetrating continua, and they are allowed to co-exist in the local volume element. Here both primary and equiaxed phases are seen as moving phases, for which corresponding velocity fields must be solved. The columnar phase is assumed to stick to the mold wall, hence no velocity field for the columnar phase is necessary. Further volume-averaged conservation equations for mass, enthalpy and species are solved for each phase. The microscopic interfacial phenomena such as grain growth and mass transfer during solidification, thermodynamic equilibrium at the interface, solute partitioning at the liquid-solid interface, drag force, etc. are taken into consideration by defining suitable closure laws. Formulations for the 3-phase approach were presented elsewhere [9-10].

Diffusion-Controlled Growth and Volume-Averaged Mass Transfer Rates

To close the mass transport equations, one needs to define the net mass transfer rate, M_{le} (or M_{lc}, kg·m^{-3}·s^{-1}), during solidification/melting. In the recent approach the morphologies for both solid phases were simplified (Fig. 1): spherical for the (globular) equiaxed grains and cylindrical for the columnar primary dendrites. Diffusion-controlled grain growth kinetics (Fig. 2) is used to define the mass transfer.

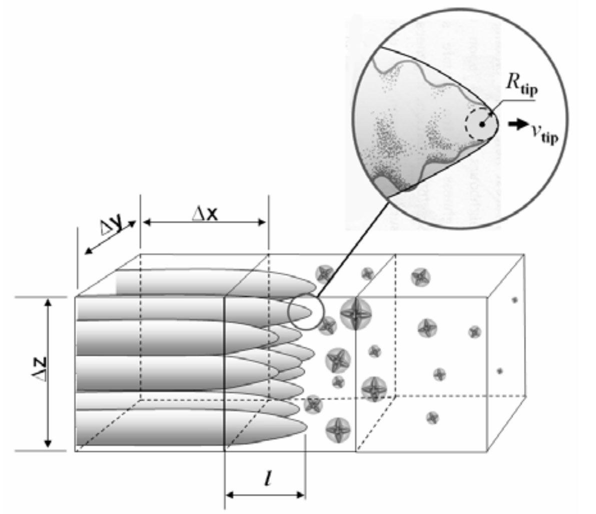

Figure 1. Schematic diagram of control volumes near columnar tip front.

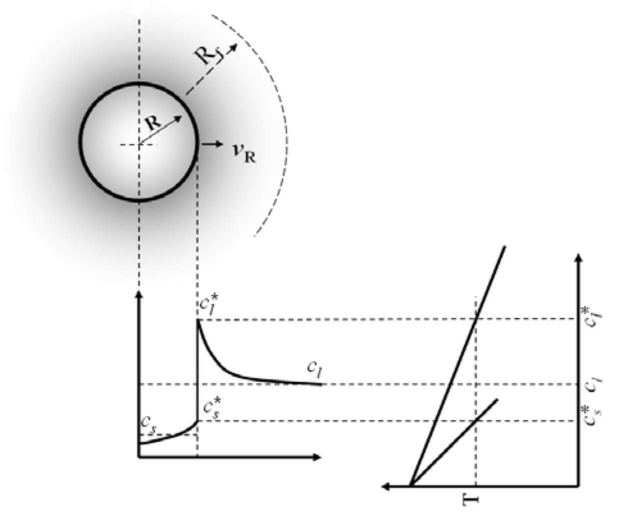

Figure 2. Diffusion-controlled crystal growth.

For the equiaxed phase the grain growth velocity, v_{R_e} (m·s^{-1}), can be solved analytically [11]

$$v_{R_e} = \frac{dR_e}{dt} = \frac{D_l}{R_e} \cdot \frac{c_l^* - c_l}{c_l^* - c_s^*} = \frac{D_l}{R_e(1-k)} \cdot \left(1 - \frac{c_l}{c_l^*}\right). \tag{1}$$

Here c_l^* (= kc_s^*) is the equilibrium liquid (solid) concentration adjacent to the solid/liquid interface which is determined by $c_l^* = (T - T_f)/m$. D_l is the diffusion coefficient in the liquid. R_e (= $d_e/2$) is the radius of the equiaxed grains. With Eq. (1), we can define the volume-averaged mass transfer rate for globular-equiaxed solidification by taking the total surface area of the spherical grains, $S_A = n \cdot \pi d_e^2$, and the Avrami-factor, f_l, to become

$$M_{le} = v_{R_e} \cdot \left(n \cdot \pi d_e^2\right) \cdot \rho_e \cdot f_l. \tag{2}$$

Here n is the grain number density, which is obtained with the help of the corresponding nucleation law and grain transport equation [6-7].

For columnar solidification 3 cases (Fig. 1) have to be distinguished: (i) volume elements which contain the columnar tips; (ii) volume elements ahead of the tips; and (iii) volume elements behind the tips. We trace the columnar tip fronts by a method described in the next section. In case of (ii), $M_{lc} \equiv 0$. For the case of (iii), a diffusion-controlled growth model around cylindrical trunks is used. The growth velocity in the radial direction of the cylindrical trunk is

$$v_{R_c} = \frac{dR_c}{dt} = \frac{D_l}{R_c} \cdot \frac{c_l^* - c_l}{c_l^* - c_s^*} \ln^{-1}\left(\frac{R_f}{R_c}\right), \tag{3}$$

where now $R_c = d_c / 2$ is the average radius of a cylindrical dendrite trunk, and $R_f = \lambda_1 / 2$ is half of the dendrite primary arm spacing, λ_1. So we can define the volume-averaged net mass transfer rate for those volume elements by taking the total surface area of columnar dendrite trunks per volume, $S_A = \pi d_c / \lambda_1^2$, and the Avrami-factor, f_l, to become

$$M_{lc} = v_{R_c} \cdot \left(\pi d_c / \lambda_1^2\right) \cdot \rho_c \cdot f_l . \tag{4}$$

For the elements containing growing columnar tips (case i), the mass transfer rate is written as

$$M_{lc} = v_{R_c} \cdot n_c \cdot \left(\pi d_c \cdot l_{ref}\right) \cdot \rho_l \cdot f_l + v_{tip} \cdot n_c \cdot \left(\pi R_{tip}^2\right) \cdot \rho_l \cdot f_l \ . \tag{5}$$

The characteristic length l_{ref} is defined in the next section. The first term on the left side of Eq. (5) denotes the mass transfer rate due to growth in radial direction, and the second term that which is due to growth in axial direction. $n_c = 4 f_c / \left(\pi d_c^2 \cdot l\right)$ is the number density of the columnar trunks per volume. The dendrite tip velocity, v_{tip}, and the tip radius, R_{tip}, are calculated according to [11-12].

<u>Columnar Tip Front Tracking Algorithm and Prediction of CET</u>

Columnar tip front tracking is based on the assumption that columnar dendrite trunks grow from the wall into the bulk melt, depending on the tip growth speed, v_{tip}. However, no growth-preferred crystalline orientation is taken into account. The following columnar tip front tracking procedure can be applied independent of the type of volume element in use (structured/unstructured, 2D/3D).

1. Each control volume element is indexed with a columnar status, i_c, which indicates whether the control volume element contains the columnar tip front ($i_c = 1$), columnar dendrite trunks ($i_c = 2$), or no trunks or tips ($i_c = 0$). All control volume elements are initialized with $i_c = 0$, except the boundary (wall) elements, which are marked with $i_c = 1$.
2. A reference length, l_{ref}, is assigned to each control volume element by seeing the control volume element as an equivalence sphere with a radius of $l_{ref} / 2$. In 3D cases the volume of the sphere must be equal to that of the corresponding control volume element: $\frac{4\pi}{3} \cdot \left(l_{ref} / 2\right)^3 = \Delta V$.
3. No preferred crystal growth orientation is predefined. The columnar front is assumed to grow parallel to the local heat flow direction with a growth velocity, v_{tip}, which is determined by the KGT model [11-12]. The actual position of the front is tracked by the integral $l = \int_t v_{tip} dt$, as soon as the front enters the control volume element.
4. As soon as l exceeds l_{ref}, the columnar tip front is thought to grow out of the supposed “tip” volume element. In this case the neighboring control volume elements, which are still indexed with $i_c = 0$, will be “reached” by the columnar tip front, and converted to $i_c = 1$, whereas the marker of the first volume element is set to $i_c = 2$.
5. A mass transfer from the liquid to the columnar phase is only taken into consideration for those control volume elements where $i_c \neq 0$.
6. For the mechanical interaction between the two solid phases a simple approach is used. Both columnar and equiaxed phases are allowed to coexist in the same volume element, even behind the columnar tip elements. When the local volume fraction of the columnar

phase, f_c , is more than a critical value, f_c^{free} (e.g. 0.2), an infinite drag force coefficient is applied in the corresponding momentum equations, and thus the equiaxed grains are "captured" by the columnar phase. When f_c is smaller than f_c^{free}, no drag force is applied.

7. The columnar tip stopping mechanism described by Hunt [13] is implemented to model the CET. In the columnar tip elements, the tip growth velocity, v_{tip} , is set to zero as soon as the local volume fraction of the equiaxed grains, f_e , exceeds the critical threshold of $f_{e,CET} = 0.49$.

Benchmark Simulation

The solidification of a binary steel ingot (Fe-0.34 wt.% C) with a relatively small size was simulated (Fig. 3). The ingot is divided into 41607 volume elements with mean grid size of 10.5 mm^3. The casting is assumed to be filled instantaneously. The initial temperature is 1785 K. The mold and surrounding air is assumed to remain at 300 K. Two heat transfer coefficients are used: $H = 700$ W·m^{-2}·K^{-1} between the casting and the mold, and 100 W·m^{-2}·K^{-1} between the casting and the air. In the simulation no shrinkage is taken into consideration, and hence a Boussinesq approximation is used to account for thermo-solutal convection and grain sedimentation. All properties and parameters used are listed in Table 1.

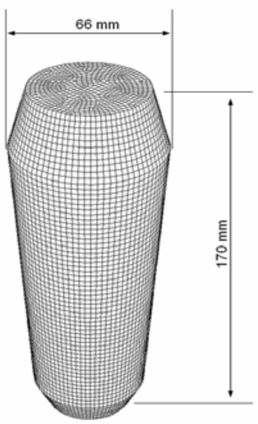

Figure 3. 3D grid used for the simulation of a steel ingot .

Table 1. Properties and parameters used in simulation

Thermo physical properties	Thermodynamic properties:
$c_{p(l)} = c_{p(s)} = 808.25$ Jkg^{-1}K^{-1}	$k = 0.2894$
$D_l = 2\text{x}10^{-8}$ m^{2}s^{-1}	$m = -8453.0$ K
$D_e = D_c = 5.6\text{x}10^{-10}$ m^{2}s^{-1}	$T_f = 1811$ K
$\Delta h_f = h_l^{ref} - h_e^{ref} = 256476$ Jkg^{-1}	$\Gamma = 2.9\text{x}10^{-7}$ mK
$k_l = k_e = k_c = 33.94$ Wm^{-1}K^{-1}	
$\beta_T = 0.0002$ K^{-1}	Nucleation parameters:
$\beta_c = 0.011$ wt.%$^{-1}$	$n_{\max} = 5.\text{x}10^9$ m^{-3}
$\rho_l = \rho_e = \rho_c = 7027$ kgm^{-3}	$\Delta T_N = 5$ K
$\Delta\rho = \rho_l - \rho_{e/c} = 294$ kgm^{-3}	$\Delta T_\sigma = 2$ K

The overall solidification sequence (Fig. 4) is dominated by heat transfer. The solidification starts as soon as the surface temperature drops below liquidus. At $t = 5$ s, the equiaxed grains nucleate near the wall, start to sink, and induce melt convection. The melt is dragged downwards along the wall by the sinking grains, which in turn induces a rising melt flow in the middle of the casting: an axis-symmetrical convection roll forms. In addition to the grain-sedimentation-induced convection, thermal and solute buoyancy also drive melt convection. Sedimentation influences the distribution of equiaxed grains. The equiaxed grains sink down, and settle in the bottom region, where the volume fraction of the equiaxed phase reaches a quite high level rather quickly. As solidification proceeds ($t = 20$ s), the volume fraction of the columnar phase (f_c) in the mold wall region increases. In addition, the equiaxed grains continue to nucleate, sink and grow. They settle and pile up in the lower region of the ingot. At $t = 20$ s, f_e in the lower part of the ingot has reached 77%, and the equiaxed grains can no longer move freely. Because f_c is also larger than f_c^{free} (=20%), they are captured and incorporated into the interdendrite region. At $t = 60$ s, the two columnar tip fronts from both sides have met in the middle of the casting. This leads to the formation of two closed columnar tip front lines: one in the upper region where the temperature is still quite high and the solid fraction is low, and the second in the lower part of the casting, where the the solidification is nearly completed, mainly with equiaxed grains ($f_e \geq 0.99$). Here, the columnar tip front in the bottom region has already been blocked by the presence of many equiaxed grains. The columnar tip fronts in the upper part are still able to move until they meet in the center of the ingot and disappear. However, in the lower part of the casting the columnar tip front has ceased to propagate further. This indicates the occurrence of a CET.

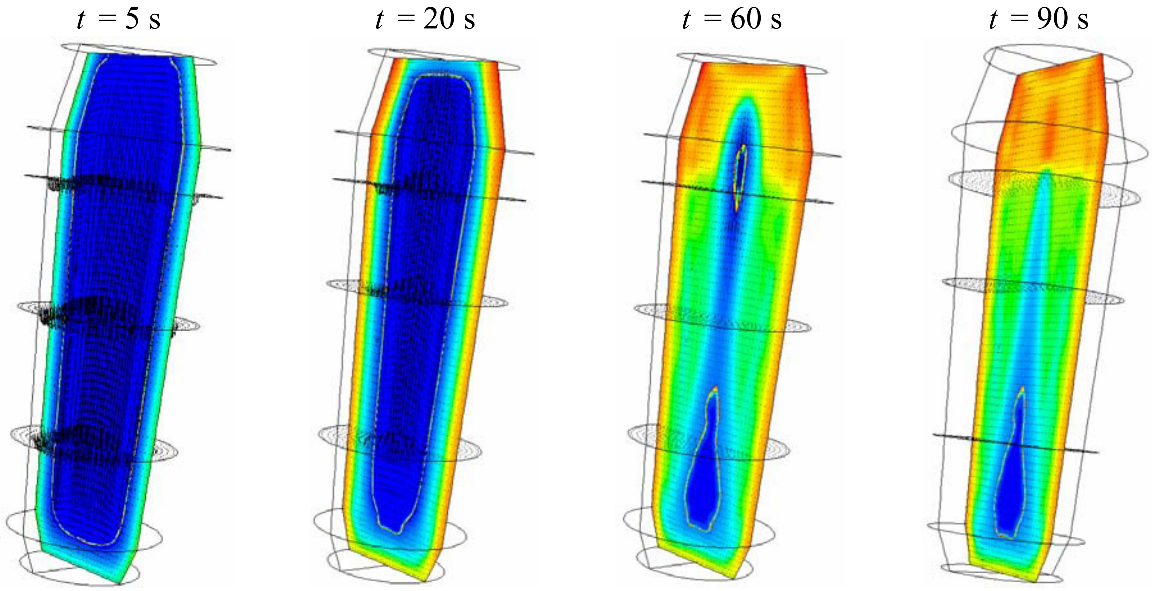

f_c (0~0.64) + $\vec{u}_l$(~0.017 ms^{-1})
f_c (0~0.98) + $\vec{u}_l$(~0.016 ms^{-1})
f_c (0~0.99) + $\vec{u}_l$(~0.0034 ms^{-1})
f_c (0~0.99) + $\vec{u}_l$(0)

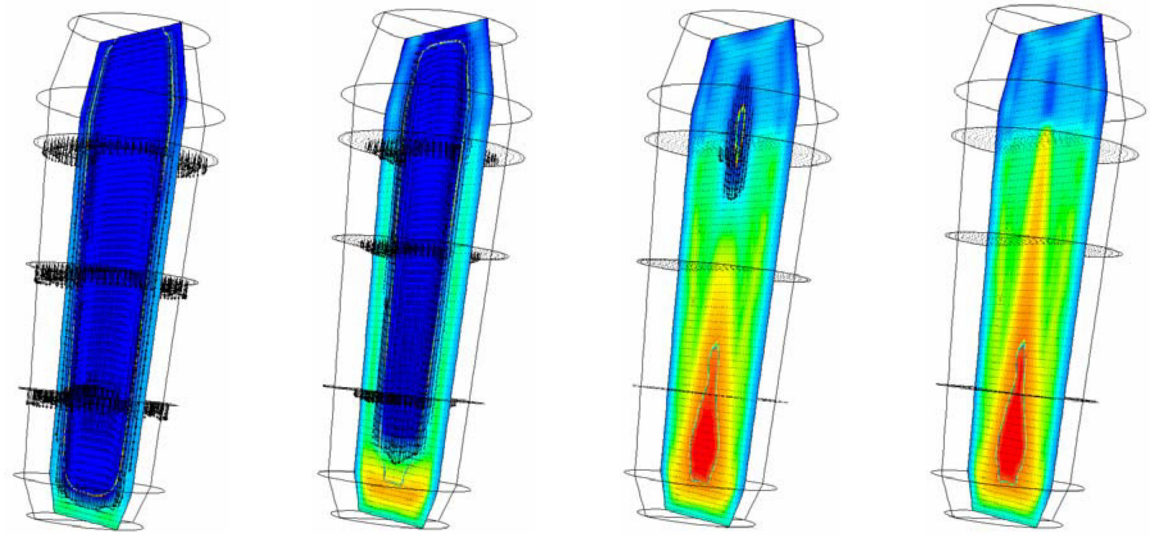

f_e (0~0.40) + $\vec{u}_e$(~0.024 ms^{-1})
f_e (0~0.77) + $\vec{u}_e$(~0.018 ms^{-1})
f_e (0~1.0) + $\vec{u}_e$(~0.010 ms^{-1})
f_e (0~1.0) + $\vec{u}_e$(0)

Figure 4. Solidification sequences of the ingot. Both f_c and f_e in the central vertical section are shown using a color scale, with red as the maximum and blue as the minimum. The velocity of the melt, $\vec{u}_l$ is shown together with f_c, while the velocity of the equiaxed grains, $\vec{u}_e$, is shown with f_e. Additionally, the velocity fields in 3 horizontal sections are also shown. The columnar tip front envelope is shown as a white line.

The results presented for the steel ingot benchmark reproduce the typical experimentally observed solidification phenomena reported often in the literature [14]. The lower cone-shaped negative segregation is caused by grain sedimentation. The positive segregation at the ingot's top is explained by the convection of segregated melt from the ingot's center. It has to be mentioned that channel segregations, which are frequently reported to occur in steel ingots, are not predicted by the presented simulation. The probable reasons are that melting (although possible) was not taken into account, and that the numerical grid used was definitely too coarse for such details [15].

The predicted macrosegregations are shown in Fig. 5. A cone-shaped negative segregation is predicted in the lower part of the ingot, where high sedimentation rates occur. The solute-poor equiaxed grains pile up at the bottom of the ingot, and the solute-rich residual melt rises. The resulting c_{mix} distribution reveals a similarity to the CET profile. The positive segregation which forms at the top part of the ingot is due to melt convection. The solute-rich melt rises as the equiaxed grains sink. The solute redistribution in the melt is strongly dependent on the melt convection. Axis-symmetrical convection rolls (Fig. 4) occur. In the casting center the rising melt transports solute-rich melt from the bottom region towards the top. As the melt hits the casting top, it diverges into side streams, which result in the specific positive segregation.

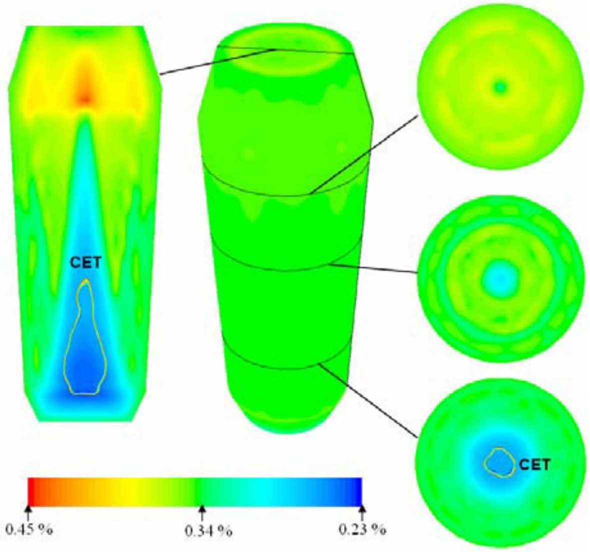

Figure 5. Predicted macrosegregations in terms of c_{mix} (wt.%C).

Comparison with Classical Analytical Solutions

In order to compare our CET predictions with classical experimental and analytic results [11, 13], a 1D directional solidification with the configuration of Fig. 6(a) was proposed. 3 phases are included, but neither flow nor feeding is taken into consideration. The physical parameters are the same as those given in Table 1. Over 20 different simulations were made by varying the process parameters (initial temperature T_0 = 1785~1805 K, wall temperature T_{w} = 300~500 K, and heat transfer coefficient at the wall H = 100 ~ 2000 $\mathrm{Wm^{-2}K^{-1}}$). As nucleation parameters we assumed $\Delta T_N = 3$ K, $\Delta T_\sigma = 1$ K, and $n_{\max} = 10^{10}\ \mathrm{m^{-3}}$. The solidification process is transient. Columnar phase grows with a tip velocity v_{tip} [11-12] unidirectionally from wall towards bulk region. The equiaxed grains nucleate and grow in front of and/or behind the columnar tips. As soon as the columnar tips are blocked by the growing equiaxed grains, we record the tip growth velocity v_{tip} and the temperature gradient G at the same moment and position to compile a CET map (Fig. 6b). Independent of the chosen parameters (T_0, T_{w}, H), all the CET points fall into the gray band, which is defined by a special relationship of log(v_{tip}) against log(G). This result coincides with the classical map [11]. When the nucleus density (n_{max}) is increased, e.g. from 10^{10} to $5\mathrm{x}10^{10}\ \mathrm{m^{-3}}$, the gray band of the CET moves towards the lower-right corner of the diagram. This also agrees with Hunt's predictions [13].

With a similar configuration of Fig. 6(a), further simulations were made to investigate the solute redistribution in the mushy zone. Here, only columnar growth (no equiaxed) was taken into consideration. In Fig. 7 the volume-averaged melt concentration, c_l , is plotted against the solid phase fraction, f_{s}, along the growth direction in the mushy zone. 3 calculated $c_l - f_s$

curves with corresponding model assumptions are presented. For curve 1 (Δ) solidification shrinkage and feeding flow were not taken into consideration, and a diffusion coefficient of $D_l = 2\text{x}10^{-8}$ m^{2}s^{-1} was used; for curve 2 (◊) solidification shrinkage and feeding flow were once again ignored, but now an artificially enlarged diffusion coefficient $D_l = 10^{-7}$ m^{2}s^{-1} was used; and for curve 3 (o) solidification shrinkage (ρ_l = 7027, ρ_l = 7324 kg.m^{-3}) and feeding flow were taken into consideration by replacing the boundary condition of a 'symmetrical plane' with a pressure inlet. It was found that the 3 calculated curves differ only slightly from the Scheil curve (□). The reason is that the Scheil model is based on the assumption of an ideal diffusion of solute elements in the liquid phase, i.e. $c_l^* \equiv c_l$, while in the recent numerical model a diffusion-controlled growth model is implemented, i.e. $c_l^* \neq c_l$. If the diffusion coefficient, D_l , were rather high, one would expect the diffusion to be very efficient, and so expect the $c_l - f_s$ curve to be close to the Scheil curve. This is proven by the simulation with the artificially enlarged D_l (curve 2). For the case in which feeding flow is taken into consideration, the segregated melt is transported along the feeding direction, thus the $c_l - f_s$ curve is shifted slightly to the upper-left of the Scheil curve. It causes macrosegregations.

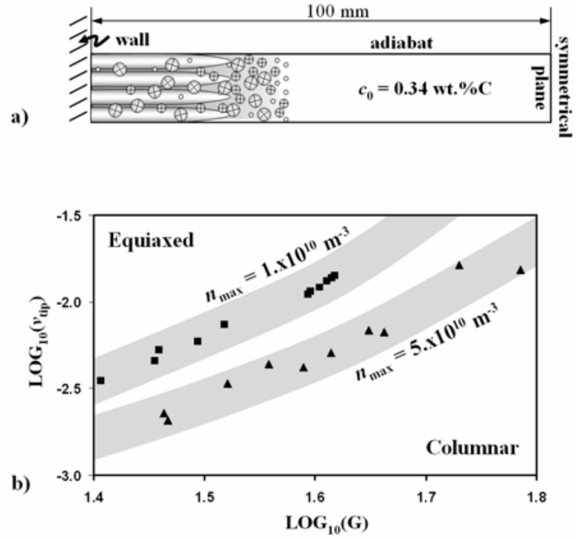

Figure 6. a) Configuration of the considered 1D benchmark; b) Predicted CET map for Fe-0.34 wt.% C.

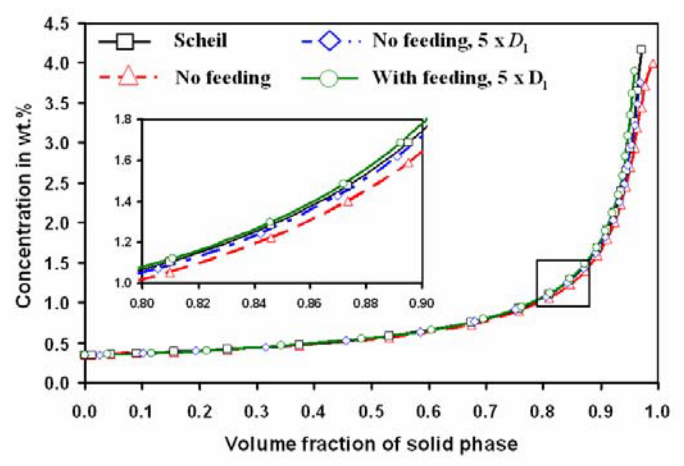

Figure 7. Solutal redistribution ($c_l - f_s$ curve) in unidirectional solidification for Fe-0.34 wt.%C.

A further 1D columnar solidification with feeding flow is simulated and compared with the analytical and experimental macrosegregation results of Flemings et al.[16] and Kato et al.[17]. As shown in Fig. 8(a), the calculated solidification sequence represents the typical situation of unidirectional solidification against a cold mold with a finite resistance to heat transfer at the metal/mold interface. According to Flemings' analytical solution, maximum positive segregation (inverse segregation) occurs on the casting surface, and slightly positive segregation occurs along the sample, almost until the end of the rod. Negative segregation can only occur at the end of solidification, when feeding is insufficient. Our 1D numerical result (Fig. 8b) agrees with these analytical and experimental findings [16-17]. Fig. 8(b) shows the c_{mix} curve for three different instants in time. Thus, the development of macrosegregation during solidification can be followed. It is interesting to see that c_{mix} near or immediately behind the columnar tip front is always lower than c_0. The reason for this is that the segregated melt from this region is transported towards the columnar root region, and so replaced by fresh melt (c_l = c_0). In the root region, however, solidification is continuously fed by highly segregated melt, and therefore c_{mix} increases and positive segregation forms.

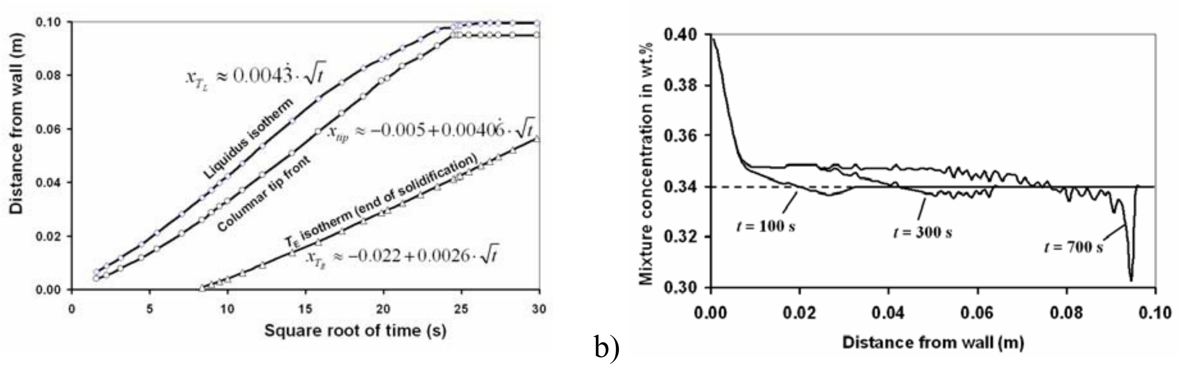

a)

b)

Figure 8. Feeding induced macrosegregation in a 1D columnar solidification. Process parameters are: initial temperature, 1785 K, wall temperature, 300 K, heat transfer coefficient at the wall, 700 $Wm^{-2}K^{-1}$. a) Calculated position of liquidus isotherm, columnar tip front and eutectic isotherm; b) Macrosegregation (c_{mix}) development at different instants in time.

Closing Remarks

A 3-phase volume averaging model for mixed columnar-equiaxed solidification was presented, which takes the following factors into consideration: the growth of columnar dendrites and equiaxed grains, the sedimentation of equiaxed grains, melt convection, the movement of the columnar tip front, the occurrence of a CET, and the formation of macrosegregations. A 3D benchmark simulation of a binary steel ingot (Fe-0.34 wt.%C) was shown. The simulation results reproduced the typical experimentally observed solidification phenomena reported often in literature [14]. The model was also evaluated by comparing it with classical analytical models based on a limited 1D situation, and satisfactory agreements were obtained.

References

1. C.Y. Wang, and C. Beckermann, *Metall. Mater. Trans.*, 25A(1994), 1081-93.
2. M.A. Martorano, C. Beckermann, and Ch.-A. Gandin, *Metall. Mater. Trans.*, 34A(2003), 1657-74.
3. Ch.-A. Gandin, T. Jalanti, and M. Rappaz, *Modeling of Casting, Welding and Advanced Solidification Processes VIII,* ed. B.G. Thomas and C. Beckermann (Warrendale, PA: TMS, 1998), 363-374.
4. Ch.-A. Gandin, and M. Rappaz, *Acta Metall. Mater.*, 42(1994), 2233-46.
5. M. Rappaz, and Ch. A. Gandin, *Acta Metall. Mater.*, 41(1993), 345-360.
6. A. Ludwig, and M. Wu, *Metall. Mater. Trans.*, 33A(2002), 3673-83.
7. M. Wu, A. Ludwig, A. Bührig-Polaczek, M. Fehlbier, and P.R. Sahm, *Inter. J. Heat Mass Transfer,* 46(2003), 2819-32.
8. M. Wu, and A. Ludwig, *Solidification and Crystallization*, ed. D.M. Herlach (Weinheim Germany: Wiley-VCH Verlag GmbH & Co. KGaA, 2004), 204-212.
9. M. Wu, and A. Ludwig, *Metall. Mater. Trans. A*, submitted (2005).
10. A. Ludwig, and M. Wu, *Mat. Sci. Eng. A*, in print (2005).
11. W. Kurz, and D.J. Fischer, *Fundamentals of Solidification*(Aedemannsdorf, Switzerland: Trans Tech Publications, 1989).
12. J. Lipton, M.E. Glicksman, and W. Kurz, *Mater Sci. Eng.*, 65(1984), 57-63.
13. J.D.Hunt, *Mater. Sci. Eng.*, 65(1984), 75-83.
14. J. Campbell, *Castings* (Oxford: Butterworth Heinemann Ltd, 1991).
15. J. Guo, and C. Beckermann, *Numerical Heat Transfer*, 44(2003), 559-576.
16. M.C. Flemings, and G.E. Nereo, *Trans. TMS-AIME*, 239(1967), 1449-61.
17. H. Kato, and J.R. Cahoon, *Metall. Mater. Trans.*, 16A(1985), 579-587.